PHYSICAL REVIEW A **88**, 033408 (2013)

Laser-controlled rotational cooling of Na_2 based on exceptional points

V. Kokoouline,[1] A. Wearne,[1] R. Lefebvre,[2,3] and O. Atabek[2,*]

[1] *Department of Physics, University of 'Central Florida, Orlando, Florida 32816, USA*

[2] *Institut des Sciences Moléculaires d'Orsay, Bâtiment 350, Université Paris-Sud (CNRS and UMR 8214), 91405 Orsay, France*

[3] *U.F.R. de Physique Fondamentale et Appliquée, Université Pierre et Marie Curie, 75321 Paris, France*

(Received 3 June 2013; revised manuscript received 18 July 2013; published 6 September 2013)

Exceptional points (EPs) corresponding to resonance coalescence (i.e., complex energy degeneracy and identical wave functions) occur in many areas of non-Hermitian physics and, in particular, in laser-induced molecular dynamics for specific choices of two control parameters. We have previously shown [Atabek, *et al.*, Phys. Rev. Lett. **106**, 173002 (2011)] how these control parameters, namely, the wavelength and the intensity of the external field, have to be tuned to take advantage of EPs for selective vibrational transfers within a reduced one-dimensional model describing a diatomic molecule with frozen rotation. Moreover, the possibility offered by such transfers to adiabatically transport all the vibrational population to the ground $v = 0$ level has been presented as a realistic vibrational cooling strategy with an entropy flow toward the field-induced dissociative channel. The purpose of the present article is twofold: (i) Extend the model to a full three-dimensional quantum description of the rotating molecule and discuss the existence, determination, and role of EPs involving rovibrational resonances; (ii) examine the possibility for a further challenging step in obtaining ultracold molecules through combined vibrational and rotational laser control dynamics, aiming at total purification for reaching the ground ($v = J = 0$) rovibrational level. The illustrative example is the Na_2 molecule for which translationally cold species have experimentally been obtained.

DOI: 10.1103/PhysRevA.88.033408 PACS number(s): 37.10.Mn, 37.10.Pq, 33.80.Gj, 42.50.Hz

I. INTRODUCTION

Molecular rovibrational cooling is a major challenge in studying small molecules at the level of individual rotational and hyperfine states with theoretical and experimental achievements aiming at their formation, deterministic manipulation, and control of their internal couplings [1,2]. In particular, a variety of robust techniques has been developed referring to blackbody-radiation-assisted lasers [3,4] or optical pumping by broadband femtosecond lasers [5]. In this context, methods involving photoassociation of ultracold atoms lead to translationally cold tightly bound molecules in a given electronic state [6]. To transfer most of these molecules to their ground vibrational state in order to achieve vibrational cooling requires additional sequences of shaped laser pulses. The next step in the search for ultracold temperatures is the rotational cooling within the rotational manifold of the vibrationless ground state.

The purpose of the present paper is to extend to a full three-dimensional quantum molecular model the adiabatic population transfer mechanism using a laser-controlled dissociation scenario based on exception points (EPs) that we have recently proposed for the vibrational cooling of a rotationless Na_2 [7]. Even more than an extension, this paper brings clear evidence that EPs in a one-dimensional context are not mathematical artifacts but have real physical existence. EPs correspond to specific laser wavelengths and intensities for which two resonances coalesce, meaning complex energy degeneracy with, in addition, identical wave functions [8,9]. Such points are rather common in non-Hermitian physics [10,11] where they may occur in many fields from optics [12] to laser physics [13], atomic and molecular physics [14,15], exciton transfers [16], and transmission in quantum dots [17]. An appealing property is that a continuously chirped laser pulse following a loop enclosing the EP leads to a permutation of the two involved resonance states [18]. This is at the origin of the strategy used in this paper to monitor the rotational transfer. In practice, translationally cold Na_2 species are prepared by photoassociation in a metastable bound state ${}^3\Sigma_u^+$, which is then considered as a ground state. The laser-controlled transfer scenario consists of applying an electromagnetic field, which couples this state to a repulsive and, thus, dissociating excited ${}^3\Pi_g$ state. Imposing a pure outgoing wave (Siegert-type) boundary condition on the wave function of this repulsive state is at the origin of non-Hermicity, and the resulting discretized resonances are identified through a series of quantized complex energies of the Hamiltonian of the field-dressed system with imaginary parts related to their dissociation lifetimes. The elementary step of the population transfer is between two adjacent resonances originating from field-free rovibrational levels $(v = 0, J + 2)$ and $(v = 0, J)$ accommodated by the bound metastable electronic state potential and radiatively coupled through the $J + 1$ dissociative potential of the excited electronic state. This step could be achieved very selectively, although it suffers a decay mechanism toward the continuum of the $J + 1$ excited state. The residual populations, after the pulse is over, could then be transferred step by step to the rotationless ground state ($v = J = 0$) either using successive pulses each enclosing a given EP or a single pulse enclosing several EPs. Contrary to a stimulated Raman adiabatic passage technique, not fully appropriate for purification purposes, the present cooling strategy involves a dissipative channel where the entropy goes [19]. But, as a consequence and for a complete implementation of the method, there remains a compromise to find in order to ensure the adiabaticity requirement of the model. A long pulse duration fulfilling adiabaticity conditions could result in the depletion of the overall molecular population through photodissociation. This

---

[*] osman.atabek@u-psud.fr

point and its consequences have to be checked carefully when appropriately shaping the control laser pulse [20]. In the following, the Na_2 molecule is taken as an illustrative yet realistic example since the formation of ultracold sodium molecules has been demonstrated in Ref. [21]. We assume that the molecule is initially prepared in its vibrationless ($v = 0$) lowest triplet electronic state $a\,^3\Sigma_u^+(3\,^2S + 3\,^2S)$, referred to as state u. The electromagnetic field with wavelengths around 550 nm couples state u with the $(1)\,^3\Pi_g(3\,^2S + 3\,^2P)$ excited electronic state, labeled g. Finally, for laser intensities in consideration (tens of $\mathrm{MW/cm^2}$), the natural spontaneous emission rate of the excited $^3\Pi_g$ state is negligible as compared to the molecular photodissociation rate.

The paper is organized as follows: The adiabatic Floquet formalism for the resonance calculation is presented within a full three-dimensional model in Sec. II. Two different approaches [discrete variables representation (DVR-) like with an absorbing potential and Fox-Goodwin with a complex coordinate] for solving the resulting close-coupled equations are compared in Sec. III. Section IV gathers the results for an accurate determination of rotational EPs, whereas, a map of clusters of EPs is displayed in Sec. V. Section VI is devoted to rotational transfer strategies using either series of pulses or single ones by comparing the relative robustness of the resulting processes. The role of adiabaticity and possible nonadiabatic contamination on population transport mechanisms is discussed in Sec. VII. Finally, Sec. VIII proceeds to a generalization of the role of EPs on observables other than energy with the important proof that the laser-induced changes in the average angular momentum may also present similar properties close to the EP.

II. THEORY: THE FLOQUET FORMALISM

We investigate the Na_2 molecule in an external laser field by solving the time-dependent Schrödinger equation (TDSE) with a Hamiltonian $H = T + V_m + V_{\mathrm{int}}$, which includes the full three-dimensional kinetic-energy term T for the rovibrational motion of the molecule, the adiabatic Born-Oppenheimer potentials V_m of the field-free molecule, and the molecule-field interaction V_{int}. We consider two Born-Oppenheimer electronic states $^3\Sigma_u^+$ and $^3\Pi_g$ correlating at large values of the internuclear distance R to the $\mathrm{Na}(3S) + \mathrm{Na}(3S)$ and $\mathrm{Na}(3S) + \mathrm{Na}(3P)$ dissociation limits (as illustrated in the inset of Fig. 1). For the sake of simplicity, we neglect the spin-orbit coupling. Actually, this would only slightly modify the positions of exceptional points in the laser parametric plane without changing the conclusions of the study. We refer to the Born-Oppenheimer electronic wave functions as ϕ_k, where k is either u or g. The laser-molecule interaction V_{int} is written in the length gauge and dipole approximation as

$$V_{\mathrm{int}} = \vec{\mu}(R) \cdot \vec{\epsilon}\mathcal{E}_0 \cos(\omega t), \tag{1}$$

where $\vec{\mu}(R)$ is the transition dipole moment between u and g states. The unitary vector $\vec{\epsilon}$ specifies the polarization direction of the external field, assumed to be linear with respect to the laboratory axis Z. The amplitude $\mathcal{E}_0$ of the electric field is constant in time or varies much slower than $\cos(\omega t)$. The wavelength $\lambda = 2\pi c/\omega$ and the intensity $I = c\mathcal{E}_0^2/8\pi$ are the laser parameters taken into consideration for the control purpose.

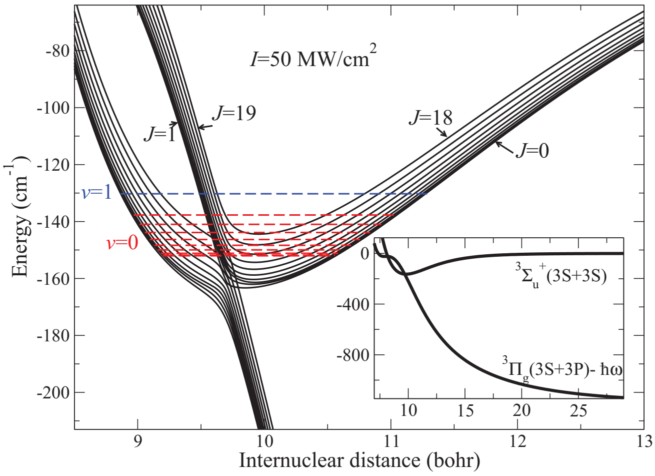

FIG. 1. (Color online) The Na_2 potential curves retained in the proposed scheme. The main figure shows the adiabatic potential curves obtained by diagonalizing the interaction potential with $J = 0,1,\ldots,19$, wavelength $\lambda = 552$ nm, and intensity $I = 50\ \mathrm{MW/cm^2}$. The energy origin is chosen at the dissociation limit of the attractive curve and corresponds to the dissociation energy of $\mathrm{Na}(^2S) + \mathrm{Na}(^2S)$ at zero intensity. Red horizontal lines indicate the positions of several rovibrational resonances for $v = 0$, whereas, the blue line shows the position of the lowest rotational level of $v = 1$. The inset displays the $^3\Sigma_u^+$ and $^3\Pi_g$ potential curves of Na_2 for zero intensity. The $^3\Pi_g$ curves are shifted down (dressed) by the energy of one photon of wavelength $\lambda = 552$ nm.

Solutions of the TDSE are obtained using the Floquet approach, which, in principle, is valid for periodic continuous-wave fields. The time-dependent wave function of the system is Fourier expanded over channels appropriate for the rovibrating diatomic molecule,

$$|\Psi_E\rangle = e^{-iEt/\hbar} \sum_{n=-\infty}^{\infty} \sum_k \sum_J \sum_\Omega \sum_M e^{in\omega t} |\phi_k\rangle |J\Omega M\rangle \times \psi_{n,k,J,\Omega,M}(R), \tag{2}$$

where E is the complex-valued Floquet quasienergy. The index n labels different Floquet components. The product $e^{in\omega t}|\phi_k\rangle|J\Omega M\rangle$ represents one of the possible photonic-electronic-rotational channels of the field-dressed Na_2 molecule, whereas, $\psi_{n,k,J,\Omega,M}(R)$'s are the unknown expansion functions (i.e., Fourier components) of $|\Psi_E\rangle$ on the orthonormal basis of these channels. The Born-Oppenheimer electronic wave functions ϕ_k, obtained for fixed internuclear distances R with no external field applied, depend on the coordinates of all electrons in the system and on R as a parameter. The rotational factor $|J\Omega M\rangle$ in Eq. (2) is an eigenstate of the rotational Hamiltonian for the field-free molecule [22],

$$\langle \alpha,\beta,\gamma | J\Omega M\rangle = \sqrt{\frac{2J+1}{8\pi^2}} \left[D^J_{M\Omega}(\alpha,\beta,\gamma)\right]^*, \tag{3}$$

where α,β,γ are the Euler angles describing the orientation of the molecule in the laboratory frame (X,Y,Z). $D^J_{\Omega M}$'s are rotational matrices (Wigner coefficients). We now proceed to a dimensionality reduction in our model in order to end up with a minimum number of channels tractable for numerical calculations but still representative of the rotational dynamics. Ω is the projection of the total angular momentum $\vec{J}$ on the molecular axis and is actually the sum of angular (Λ) and spin (Σ) parts: $\Omega = \Lambda + \Sigma$. In the following, only the spin $\Sigma = 0$ component of the two triplet states u and g is retained, resulting in $\Omega = \Lambda$ with $\Lambda = 0$ for ${}^3\Sigma_u^+$ and $\Lambda = \pm 1$ for ${}^3\Pi_g$, respectively. Moreover, for the ${}^3\Pi_g$ state, one among the two components is left. Finally, we take into account only two different electronic states k with a single Λ value in each case ($\Lambda_u = 0$ for $k = u$ and $\Lambda_g = 1$ for $k = g$). As such, Λ is one of the relevant quantum numbers for state ϕ_k. M is the projection of J on the laboratory axis Z. Because this projection is conserved, if the laser polarization is along Z, we can set $M = 0$ without loss of generality. Finally, the two sums over Ω and M in Eq. (2) are discarded: the sum over k already accounting for the one over Ω and the sum over M being limited to $M = 0$.

The laser-molecule interaction [Eq. (1)] can also be written in scalar form as

$$V_{\text{int}} = \mu_Z(R)\mathcal{E}_0 \cos(\omega t), \tag{4}$$

with μ_Z as the appropriate component of the transition dipole on the laboratory Z axis. The frame transformation leads to the following expression for μ_Z [22] (angles α,β,γ are omitted for simplicity):

$$\mu_Z = D^{1*}_{00}\mu_z + D^{1*}_{01}\left(-\frac{\mu_x + i\mu_y}{\sqrt{2}}\right) + D^{1*}_{0-1}\left(\frac{\mu_x - i\mu_y}{\sqrt{2}}\right), \tag{5}$$

where μ_k with $k = x,\ y$, or z are the appropriate components of the transition dipole in the molecular frame (xyz). For Na$_2$, between the two electronic states ${}^3\Sigma_u^+$ ($\Lambda = 0$) and ${}^3\Pi_g$ ($\Lambda = \pm 1$), due to selection rules only, $\mu_x \equiv \mu(R)$ is not zero. In addition, while only retaining $\Lambda_g = +1$, our model allows the transition to the ${}^3\Pi_g^+$ component of the two possible (e,f) states involved in these transitions,

$$(e,f) = 1/\sqrt{2}\left[{}^3\Pi_g^+ \pm {}^3\Pi_g^-\right]. \tag{6}$$

Finally, the last two terms of the right-hand side of Eq. (5) are summed up using the identity $D^{1*}_{0-1} = D^1_{01}$.

Using the form [Eq. (2)] of the wave function, the TDSE is recast, through the Floquet formalism, in terms of the following representative set of coupled equations with, as solutions, the unknown functions $\psi_{n,k,J,\Omega,M}(R)$ [23] (in the discussion below, we will omit indices Ω and M because $M = 0$ and Ω is determined by k for the system under consideration),

$$\begin{aligned}
&\left(-\frac{\hbar^2}{2\mathcal{M}}\frac{d^2}{dR^2} + V_g(R) + \frac{\hbar^2}{2\mathcal{M}}\frac{J(J+1)-\Lambda_g^2}{R^2} + n\hbar\omega - E\right)\psi_{n,g,J}(R)\\
&\quad = \frac{\mathcal{E}_0}{2}\mu(R)\sum_{J'}\frac{\sqrt{(2J'+1)(2J+1)}}{8\pi^2}\langle D^{J'}_{00}|D^1_{01}|D^J_{01}\rangle[\psi_{n-1,u,J'}(R) + \psi_{n+1,u,J'}(R)]\\
&\left(-\frac{\hbar^2}{2\mathcal{M}}\frac{d^2}{dR^2} + V_u(R) + \frac{\hbar^2}{2\mathcal{M}}\frac{J(J+1)-\Lambda_u^2}{R^2} + n\hbar\omega - E\right)\psi_{n,u,J}(R)\\
&\quad = \frac{\mathcal{E}_0}{2}\mu(R)\sum_{J'}\frac{\sqrt{(2J'+1)(2J+1)}}{8\pi^2}\langle D^{J'}_{01}|D^1_{01}|D^J_{00}\rangle[\psi_{n-1,g,J'}(R) + \psi_{n+1,g,J'}(R)].
\end{aligned} \tag{7}$$

In the above equation, $\mathcal{M}$ is the reduced mass of Na$_2$. The photon absorption selection rules result in $J' = J \pm 1$. Once again, we stress that this is a representative set of equations reducing the description to the minimum number of channels needed for the rotational degrees of freedom. The wave functions $\psi_{n,k,J}(R)$ describing these channels are called diabatic as they are obtained from the coupled equations involving field-dressed potentials, which usually cross each other. A linear transformation yields [24] the so-called adiabatic channel functions, associated with the adiabatic potentials, which are precisely the ones illustrated in Fig. 1 for the first 20 rotational states, coupled by a 552-nm laser field of intensity $I = 50$ MW/cm^2.

III. METHODOLOGY

The system of Eq. (7) is solved numerically using two different numerical methods either DVR-like with an absorbing potential or Fox-Goodwin with a complex coordinate. The Born-Oppenheimer potentials $V_u(R)$ and $V_g(R)$ are taken from Ref. [25], and the electronic transition moment $\mu(R)$ is taken from Ref. [26]. Due to the presence of the external laser field, the system does not have purely bound rovibrational levels but resonances with finite photodissociation lifetimes. These are obtained by imposing Siegert outgoing boundary conditions resulting in non-Hermicity and quantized complex eigenenergies. Accordingly, the two employed numerical methods account for the outgoing dissociation flux through a mathematical trick (complex absorbing potential or complex coordinate) and transform the otherwise asymptotically increasing resonance wave functions into square-integrable ones.

The first method is a DVR method with an absorbing potential placed in the asymptotic region of the internuclear distances in order to absorb the outgoing dissociation flux. The method is described in detail in many references, see, for instance, Refs. [27,28]. Here, we use the version given in Refs. [29,30]. The Schrödinger equation of the problem written in the close-coupled form of Eq. (7) is a one-dimensional (along R) multichannel eigenvalue problem. In the DVR method, the eigenvalues and eigenstates are obtained by a diagonalization of the Hamiltonian matrix. To represent the Hamiltonian in a matrix form, one chooses a set of basis functions depending on R. The basis functions are such that all potentials and R-dependent couplings are diagonal over the DVR basis functions. However, the kinetic-energy term is represented by a full matrix (its actual form can be found in Refs. [29,30]).

In typical calculations, we use about 180 DVR basis functions. The number of channels is given by the product of the number of Born-Oppenheimer states (two in our case), the number of Floquet blocks (two in our case), and the number of rotational states. In most cases presented in this paper, we include values of J from 0 up to 9. Therefore, the number of channels in a typical calculation is 40. Due to the symmetry of the total Hamiltonian with respect to an exchange of the nuclei, there are two types of wave functions, symmetric S and antisymmetric A. The channel functions also have this symmetry. Each channel function is symmetric or antisymmetric under the nuclei exchange depending on J and the parity (g or u) of the electronic state. A channel function changes sign under the nuclei permutation if $A = (-1)^{\sigma+J} = -1$ ($\sigma = 1$ for ${}^3\Sigma_u^+$ and $\sigma = 0$ for ${}^3\Pi_g$) and does not change sign if $S = (-1)^{\sigma+J} = 1$. Therefore, the set of 20 S channels is completely decoupled from the one of 20 A channels. Accounting for 180 DVR basis functions along the R variable, the size of the S- or A-symmetry Hamiltonian matrix amounts to 3600. Due to the complex absorbing potential placed in the asymptotic region of R, the Hamiltonian matrices are symmetric but not Hermitian. In addition, they are sparse. As stated previously, a channel with a given J is coupled to channels with $J' = J \pm 1$ only. In numerical calculations, we use the ARPACK suite of programs [31], specially adapted for this kind of problem. Because we have to perform hundreds of diagonalizations for different values of the laser wavelength λ and intensity I, the use of sparse matrix diagonalization procedures is found to be very useful. For a given pair of parameters (λ and I), the diagonalization of the A and S blocks of the Hamiltonian matrix gives eigenenergies and wave functions for all photodissociation states that could be represented within appropriate numerical accuracy in the chosen interval of variation in R. Resonances with energies close to the dissociation limit $3S + 3S$ may not be well represented if the R interval is not large enough, but we are not particularly concerned about them. The quasienergies E of the obtained eigenstates are complex $E = E_r - i\Gamma/2$, where E_r and Γ are the energy and the width of the photodissociation resonance.

An alternate method for the accurate calculation of resonance energies and wave functions is the use of the complex rotation of coordinate R [24,32,33], which actually plays the role of the absorbing potential. In order to solve Eq. (7), the Fox-Goodwin propagation algorithm [34] is used in conjunction with a properly chosen set of imposed boundary conditions, which accounts for the correct behavior of the channel wave functions both at short and at long distances. The algorithm consists of an iterating sequence of two steps [33]: (i) properly initialized Fox-Goodwin matrices are constructed at each point of a grid (along R) in terms of independent solution matrices propagated inward and outward; (ii) the criterion for convergence is a condition to be fulfilled for matching both the functions and their derivatives on a given point of the grid. Whereas, regularity [$\psi(R = 0) = 0$] is imposed at the origin for both open and closed channels, which are classically forbidden, the boundary conditions for large R are different for these two types of channels. Zero initialization is still valid for closed channels, but Siegert-type outgoing boundary conditions should be adopted for the open ones [35]. The most important observation is that the use of the complex coordinate brings the outgoing asymptotic behavior to regularity (zero inward initialization) [33]. Such imposed boundary conditions are at the origin of quantization conditions leading to discrete complex resonance energies. In practice, starting from an initial guess for the energy, the propagation-matching procedure leads to accurate eigenenergies when properly converged.

The two methods can be worked out in a complementary way. A first guess for all resonances obtained from the DVR-type matrix diagonalization may be used as an input for the shooting procedure of the external complex scaled Fox-Goodwin method for an accurate determination even in extreme cases of very short-lived resonances [36,37]. The use of the complex absorbing potential or the complex coordinate results in a symmetric but non-Hermitian Hamiltonian and, correspondingly, a symmetric and non-Hermitian Hamiltonian matrix in the DVR method: $H_{ij} = H_{ji}$. This leads to the necessity of using a modified version of the scalar product (non-Hermitian c product [32]), which does not change if left and right vectors are exchanged $(v|w) = (w|v)$ for any state in the relevant vector space.

If this scalar product is used to calculate the expectation value $(v|\hat{O}|v)$ of an observable $\hat{O}$, it will give, in general, a complex value. Such a scalar product is used below to calculate the averaged value of J: Because different values of J are mixed by the laser field, the value $(v|J|v)$ will provide information about how strong the mixing is for eigenstate v.

IV. ACCURATE DETERMINATION OF ROTATIONAL EPs

The accurate determination of rotational EPs is far from being an easy task due to the high density of rotational manifolds for a given vibrational level, especially for a heavy diatomic, such as Na_2. Moreover, the specific three coupled channels structure ($u, J \rightarrow g, J+1 \rightarrow u, J+2$) accommodating the two resonances, which are expected to coalesce for the EP parameters, leads to field-dressed potentials with two avoided curve-crossing situations. The consequence is that, contrary to what we have while determining vibrational EPs involving but a single avoided curve crossing, a clear guide in terms of Feshbach- and shape-type resonances exchange, which greatly helps in an approximate determination of EP parameters, is now missing [7,38]. This is why we have to proceed through a complete two-dimensional (λ, I) scanning for the rotational EPs localization. For such a task, it turns out that a DVR-type method is better adapted. Figure 2 provides an example of degeneracy for rotational resonances. The variation in resonance energies (real parts only) for a series of lowest vibrational levels as a function of intensity I for $\lambda = 552$ nm is displayed in panel (a). This laser wavelength results from a

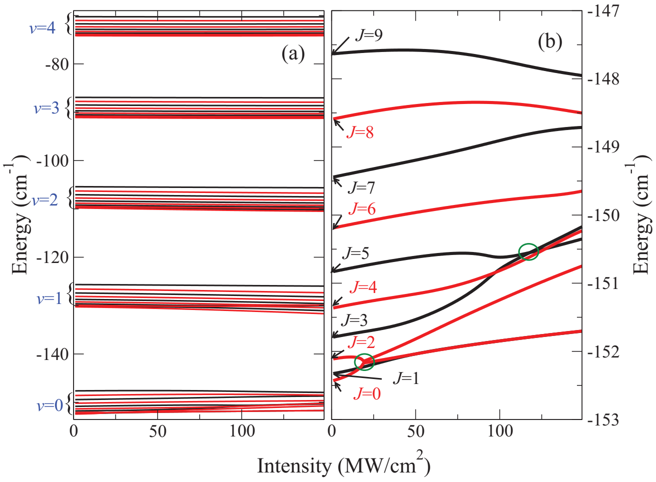

FIG. 2. (Color online) Real parts of resonance energies originating from the lowest rovibrational levels ($v = 0{-}4, J = 0{-}9$) of Na$_2$ as a function of laser intensity (panel a). The laser wavelength is $\lambda = 552$ nm. Panel (b) is a zoom within the rotational manifold of the $v = 0$ state. Red and black solid lines correspond to resonances originating from even and odd rotational levels, respectively. The circles indicate possible resonance coalescence between either even J's ($J = 0,2$) or odd ones ($J = 3,5$).

previous analysis based on a large-scale two-parameters scan, covering a region extending from $\lambda = 550$ to 556 nm and from $I = 0$ to 200 MW/cm^2. Panel (b) is a zoomed version showing the rotational structure of the $v = 0$ level. Intensities less than 200 MW/cm^2 are not large enough to mix the vibrational levels, although rotational resonances are mixed even for these modest intensities. Because the Hamiltonian is invariant under permutation of the two nuclei, transitions between even and odd J's within the same electronic state are forbidden. In the absence of the laser field, J becomes a good quantum number as indicated in panel (b). In the field-free situation ($I = 0$), the rotational energies scale with J as expected, i.e., are proportional to $J(J+1)$.

The results displayed in Fig. 3 constitute a full check of the presence of a rotational EP for a pair of rotational levels $J = 0$ and $J = 2$ taken in the $v = 0$ manifold. The coalescence is evidenced by the equality of both the real and the imaginary parts of the resonance energies originating from $J = 0$ and $J = 2$. The behavior of resonance $J = 4$ is also given to show that it merely acts as a spectator. To seek a clearer graphical illustration, the imaginary parts (very close to each other in the vicinity of the EP) are actually recast into a reduced half-width $\Gamma/2I$. The laser intensity regime is modest enough to still act as a perturbation leading to linearly behaving widths, except close to the EP. It is worth noting that, on the accurate position of the EP ($\lambda^{\mathrm{EP}} = 552$ nm, $I^{\mathrm{EP}} = 20$ MW/cm^2), both the energies and the reduced widths are exchanging with a vertical tangent as expected from the general theory of EPs [39].

V. MAP FOR CLUSTERS OF ROTATIONAL EPs

For a given pair of resonances, one may expect several EPs at different wavelengths as previously observed in cases of coalescence among resonances originating from different vibrational levels [40]. An important issue for control scenarios is to refer to an extended map of EPs, at least, within a given window in the wavelength-intensity plane. We proceed through a scan in a region of wavelength covering 6 nm between $\lambda = 550$ and $\lambda = 556$ nm and intensities up to $I = 200$ MW/cm^2, involving about eight rotational levels (from $J = 0$ to $J = 7$). Figure 4 displays the resulting EPs. In conformity with previous observations concerning vibrational resonances, EPs involving rotational pairs (J,J') appear to be organized in terms of clusters [40]. In the following, they are noted as EP(J,J'), J and J' being the corresponding rotational quantum numbers. One can roughly identify three clusters; namely, (i) EP(0,2), EP(1,3), EP(2,4), and EP(3,5)

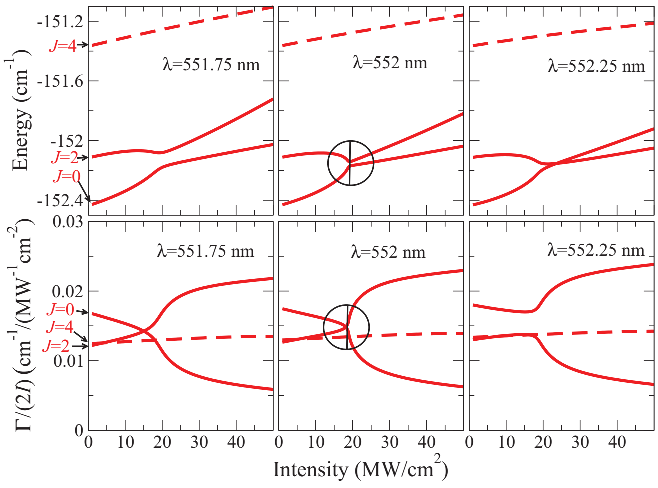

FIG. 3. (Color online) Accurate determination of the resonance coalescence $J = 0$ and 2 at wavelengths in the vicinity of 552 nm. The upper panels give the energy positions, whereas, the lower panels display the reduced half-widths as a function of intensity. The circles indicate the accurate position of the EP with the expected vertical tangent, a specific signature of its morphology. The dashed lines represent the behavior of the resonance associated with $J = 4$.

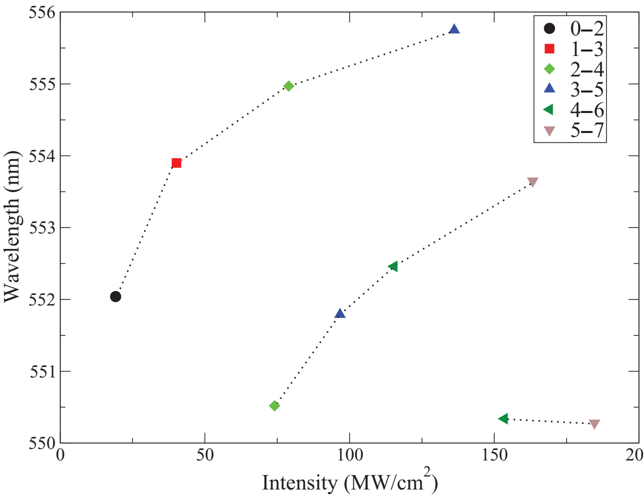

FIG. 4. (Color online) Clusters of rotational EPs in the laser parameter (wavelength-intensity) plane. The EPs are symbolized as single points in the parameter plane by the colored solid objects (dots, squares, diamonds, and triangles). The black dotted lines are drawn to guide the eyes in identifying the three clusters.

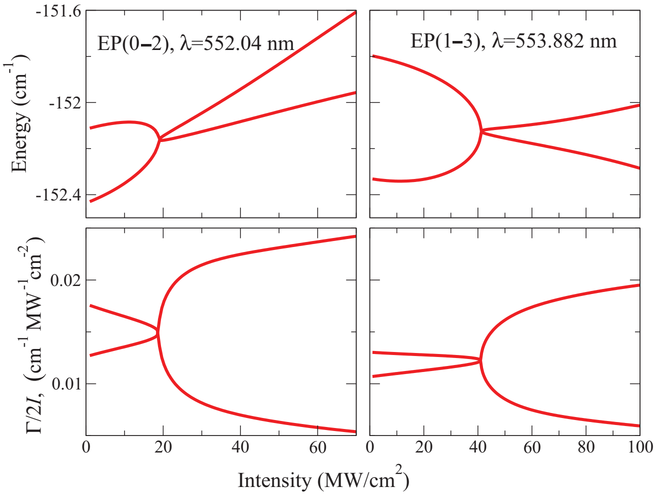

FIG. 5. (Color online) Characteristic resonance behavior close to the two EPs of Fig. 4 (black solid dot and red solid square). The left column is for EP(0,2), and the right column is for EP(1,3).

at higher wavelengths and lower intensities, (ii) EP(2,4), EP(3,5), EP(4,6), and EP(5,7) at lower wavelengths and higher intensities, and (iii) EP(4,6) and EP(5,7) at even higher intensities.

For completeness, in Fig. 5, we fully analyze the characteristic behavior of the energies and reduced half-widths of the coalescing resonances in the neighborhood of the two EPs taken from the first cluster involving either even ($J = 0{-}2$) or odd ($J = 1{-}3$) rotational resonances.

VI. ROTATIONAL TRANSFER STRATEGIES

A typical analysis of the adiabatic transfer strategy when encircling a single EP is given in Fig. 6 using a 12.5-ps-long pulse. By adiabatic, we mean, hereafter, the following of a single pair of resonances, an approximation which may induce some limitations to be carefully controlled as discussed in the next section. The parametric analytical form taken for the laser pulse is as follows:

$$\begin{aligned}\lambda &= \lambda_m + \delta\lambda\,\sin[\zeta(t)],\\ I &= I_m \sin[\zeta(t)/2],\\ \zeta(t) &= 2\pi t/T_{\max},\end{aligned} \tag{8}$$

where λ_m is close to the EP wavelength, I_m is the maximum peak intensity (larger than the one of the EP), and $T_{\max}$ is the total pulse duration. Starting from the field-free state $J = 2$ and adiabatically following the resonance labeled $J = 2$ (indicated by the trajectories in the right column), the selective transfer obtained by encircling EP(0,2) leads, at the end of the pulse, to the field-free rotational state $J = 0$. It is important to emphasize that the resonance, which is followed, is the one labeled by the initial state ($J = 2$), although this resonance switches on the one originating from $J = 0$ while encircling the EP. This is given in the energy (real and imaginary parts) versus time plane by the red trajectories. The laser loop is followed clockwise (as indicated by the arrow) to achieve better robustness in relation with Feshbach-type (i.e., narrow width) versus Shape-type (i.e., large width) resonances, which are followed [38]. Finally, the survival probability when the pulse is switched off amounts to 0.65, which is a quantitative measure of the robustness, only 35% of the initial population has dissociated.

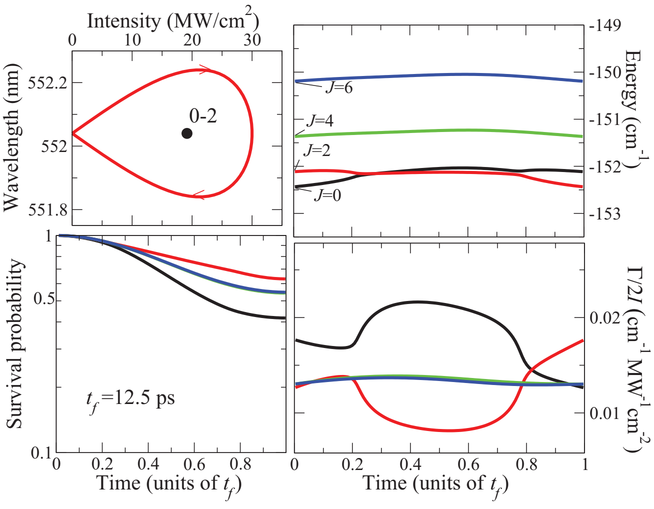

FIG. 6. (Color online) Rotational transfer encircling EP(0,2) with a chirped pulse of total duration 12.5 ps. The loop is followed clockwise (upper left panel). The resonance trajectories for $J = 0,2,4,6$ are displayed in the right column. The transfer involves a cooling scheme $(v = 0, J = 2) \rightarrow (v = 0, J = 0)$ with survival probabilities indicated in the lower left panel.

We are studying two transfer strategies [38], either based on single EPs using two successive laser pulses, namely, from $(v = 0, J = 4)$ to $(v = 0, J = 2)$ and then from $(v = 0, J = 2)$ to $(v = 0, J = 0)$ or on two successive EPs, namely, from $(v = 0, J = 4)$ to directly $(v = 0, J = 0)$ using a single laser pulse. For doing so, we have to consider pulses of equal total duration and long enough for ensuring adiabaticity. In the case of single EPs, two pulses have to be applied to successively reach $J = 4 \rightarrow 2 \rightarrow 0$, reducing the survival probability. In the case of multiple EPs, a single pulse is enough for the direct transfer $J = 4 \rightarrow 0$. This strategy is shown to be more robust with a much better final survival probability.

Figure 7 illustrates the first strategy based on two EPs using two laser pulses of both 12.5-ps duration and encircling, successively, EP(2,4) and EP(0,2), such as to realize a two-step cooling process from 4 to 2 and then from 2 to 0. For the first pulse, the initial field-free level is $J = 4$. The resonance that is adiabatically followed is $J = 4$, ending up in level $J = 2$, whereas, the laser loop encircles the EP(2,4) as indicated in Fig. 7, upper panel. The survival probability for this process is 0.3 (green line in Fig. 7, lower panel). For the second pulse, encircling EP(0,2), the starting level is $J = 2$, which is transported on the resonance labeled $J = 2$ and ends on the field-free level $J = 0$. The cumulative survival probability is given by the green curve of Fig. 7, lower panel and amounts, at the end of the second pulse, to 0.17. In other words, for this two-pulse strategy, the rotational cooling process from $J = 4$ to $J = 0$ operates with a robustness of 0.17, that is, with 17% of the total population left nondissociated.

Figure 8 illustrates the second strategy taking advantage of multiple EPs. More precisely, it concerns a rotational transfer based on a cluster of two EPs ensuring with a single laser

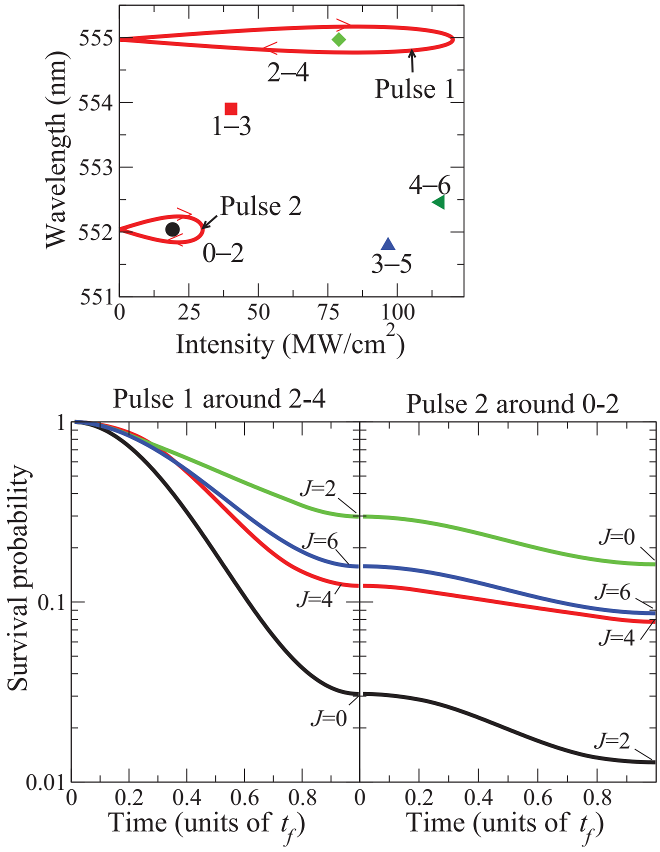

FIG. 7. (Color online) Rotational transfers based on two EPs using two laser pulses of both 12.5-ps duration and encircling, successively, EP(2,4) and EP(0,2) (upper panel). The green solid line indicates the time-dependent survival probability starting from $J = 4$ and adiabatically following this resonance. The lower panel displays the survival probabilities for the resonances $J = 0$ (black solid line), $J = 2$ (red solid line), and $J = 6$ (blue solid line). The labeling J corresponds to the final field-free state which is reached. For the first pulse, $J = 4$ and $J = 2$ are exchanging their labels, whereas, $J = 0$ and $J = 6$ are spectators. For the second pulse, it is $J = 2$ and $J = 0$, which are exchanging labels, whereas, the spectators are $J = 4$ and $J = 6$.

pulse a direct cooling from $(v = 0, J = 4)$ to $(v = 0, J = 0)$. The green solid curve displays the energy trajectories (real and imaginary parts) of the resonance $J = 4$ as a function of time. At the end of the pulse, $J = 4$ ends in the field-free state $J = 0$ with a robustness of 0.35, that is, with 35% of nondissociated molecules. In conclusion, we show that a single laser pulse of total duration 12.5 ps with a loop encircling both EP(2,4) and EP(0,2) leads to a more robust $J = 0$ population (by a factor of about 2) than two successive pulses of the same 12.5-ps duration. Both are achieving a two-step cooling process by successively encircling EP(2,4) and EP(0,2).

VII. ROLE OF ADIABATICITY ON TRANSPORT MECHANISMS

Figure 9 shows resonance trajectories in the complex energy plane when using the laser pulse of Fig. 6 encircling EP(0,2). As is also clear from Fig. 6, lower panel, the two resonances originating from field-free rovibrational states $(v = 0, J = 0)$ or $(v = 0, J = 2)$ display trajectories with well-marked differences with respect to their widths. More precisely, the resonance resulting from $J = 0$ is more than four times broader at midpulse intensities than the one resulting from $J = 2$. This is in relation with shape- versus Feshbach-type behavior as has been discussed in simpler two-channel avoided-crossing situations [38]. The higher energy $J = 2$ resonance is temporarily trapped on some upper adiabatic binding potentials, whereas, the lower energy $J = 0$ resonance is in an above-barrier tunneling position on a lower adiabatic potential. As the laser loop is encircling EP(0,2), resonances are exchanging their labels. The trajectory starting from state

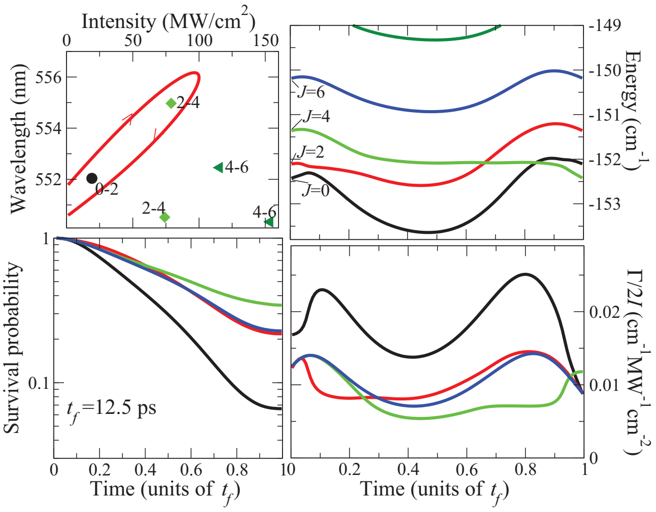

FIG. 8. (Color online) Same as in Fig. 6 but for rotational transfers based on a cluster of two EPs ensuring with a single laser pulse a direct cooling from $(v = 0, J = 4)$ to $(v = 0, J = 0)$. The total pulse duration is 12.5 ps, leading to a robustness of 0.35.

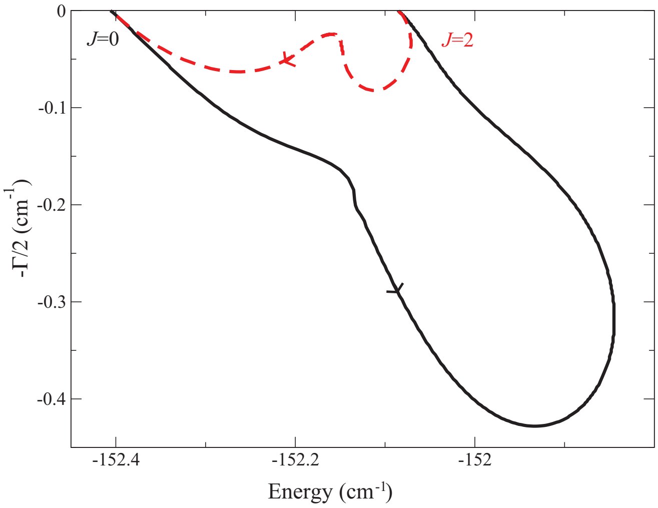

FIG. 9. (Color online) Resonance trajectories in the complex energy plane. The coordinate system corresponds to imaginary versus real parts of the energies as obtained following the laser pulse of Fig. 6 encircling EP(0,2). The solid black line is for the shape-type resonance originating from $J = 0$, and the dotted red line is for the Feshbach-type one from $J = 2$. The arrows indicate the directions which are followed.

$J = 0$ (or $J = 2$) ends up on state $J = 2$ (or $J = 0$) as expected. The difference in behavior is in the robustness of the sweeping process with respect to photodissociation. The survival probabilities when the pulse is switched off, as obtained from Fig. 6, are 0.17 and 0.40 for $J = 0$ and $J = 2$, respectively. For a purely adiabatic transport (involving very long pulse durations) where only a single resonance is followed, the sweeping process is selective and reversible from $J = 0$ to $J = 2$ or the contrary. But due to population lost during dissociation, the rotational cooling process from $J = 2$ to $J = 0$ is about two times more robust than the reverse heating one from $J = 0$ to $J = 2$. However, it is worthwhile noting that the robustness of the $J = 0$ to $J = 2$ transfer can, at will, be improved by a counterclockwise following of the laser loop of Fig. 8 by taking $\delta\lambda < 0$ in Eq. (8). This merely exchanges the roles of shape- and Feshbach-type resonances as has been proven in Ref. [20].

Long-lasting pulses, required for full adiabatic transports, would, unfortunately, bring, as a consequence, the depletion of rovibrational populations. This is why a compromise is looked for, allowing some nonadiabaticity (resonance mixing), which is merely unavoidable for laser parameters close to an EP, whatever the pulse duration. More precisely, within a two-by-two subspace involving the resonances $J = 0$ and $J = 2$, we have to consider contamination effects that have already been discussed in the recent literature [41–43]. Starting from a field-free initial state $J = 0$, the resulting resonance is not robust and actually decays with high rates (Γ's on the order of 0.8 cm^{-1} as compared to even smaller rotational energy separations). For a long enough pulse, there is no population left after following this resonance. But due to nonadiabaticity, we have to consider contamination from the resonance originating from $J = 2$. This resonance follows a trajectory, which is robust (Γ's on the order of 0.15 cm^{-1}), and due to the presence of EP(0,2), it jumps on $J = 0$. To summarize, as a consequence of nonadiabaticity in the transport process, the sweeping from $J = 0$ to $J = 2$ would require severe compromises in the pulse shaping. On the contrary, the reverse process is very easy to observe due to the robustness of the resonance originating from $J = 2$ and transforming into $J = 0$ in the vicinity of EP(0,2). The population is well transferred from $J = 2$ to $J = 0$. To be complete, we also have to consider the unavoidable contamination with the resonance originating from $J = 0$. But once more, due to its lack of robustness, this last resonance will decay fast enough to be neglected in the overall population transfer dynamics. In conclusion, if the ultimate control target is molecular rotational cooling, the necessary compromises in the adiabaticity versus robustness scheme turn out to be reachable as has recently been shown in the context of vibrational cooling of H_2^+ with 20% of the final population nondissociated [20]. Transposing from H_2^+ to Na_2, it is worthwhile noting that pulse-shaping parameters (total durations and peak intensities) are on the order of magnitudes more adiabatic in the case of Na_2, clearly supporting the analogy and advocating for an even better robustness for Na_2. If it is the reversibility in the sweeping process, which is looked for as, for instance, in the design of molecular machines for logical operation purposes [44], appropriately combining clockwise and counterclockwise pulses, there is still optimal pulse-shaping possibilities for acceptable robustness.

VIII. ROLE OF EXCEPTIONAL POINTS ON OTHER OBSERVABLES

In the presence of a laser field linearly polarized in the laboratory frame along the Z axis, the angular momentum J of the system is not conserved. For a given quasistate of Eq. (2), a convenient measure of how strongly different J's are mixed is given by the average value of $\vec{J}^2$. This average is calculated using the same scalar product as the one used for the normalization. Because the time-dependent wave function of the system is written as an expansion [Eq. (2)] over the eigenstates of the operator $\vec{J}^2$ for which

$$\vec{J}^2|\phi_k\rangle|J\Omega M\rangle\psi_{n,k,J}(R) = \hbar^2 J(J+1)|\phi_k\rangle|J\Omega M\rangle\psi_{n,k,J}(R), \tag{9}$$

the average value of $\vec{J}^2$ for $t = 0$ is given by

$$(\Psi_E|\vec{J}^2|\Psi_E) = \hbar^2 \sum_{n,k,J} \int dR[\psi_{n,k,J}(R)]^2 J(J+1). \tag{10}$$

For better readability and labeling at $t = 0$, it is more convenient to use the averaged value of the quantum number J rather than $\vec{J}^2$,

$$(\Psi_E|J|\Psi_E) = \sum_{n,k,J} \int dR[\psi_{n,k,J}(R)]^2 J\,. \tag{11}$$

This quantity gives the magnitude J of the angular momentum for rotational states of the molecule for $I = 0$ [in contrast to the value of $\hbar^2 J(J+1)$ if Eq. (10) is used]. For $I > 0$, similar to the quasienergies, the average value of J is, in general, a complex number. Figure 10 shows the behavior of $(\Psi_E|J|\Psi_E)$ close to EP(0,2) for the four lowest resonances (originating from $J = 0,2,4,6$) of the even J network. Once again, at field-free conditions, these averages actually correspond to the values of the rotational quantum numbers J. Here again, one clearly observes a bifurcation scenario between the trajectories

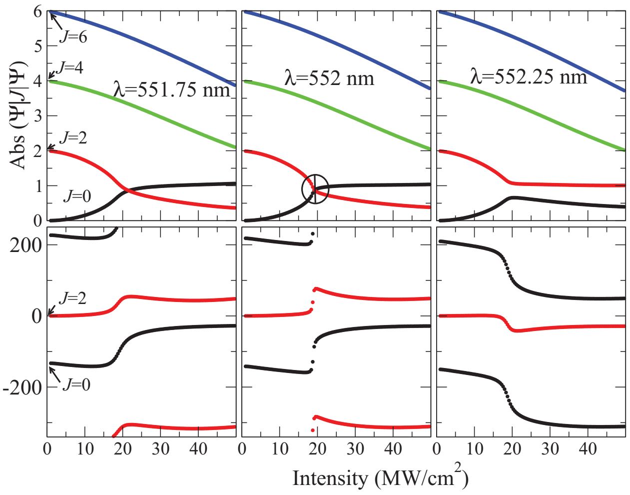

FIG. 10. (Color online) Behavior of the averaged value of J on the four lowest resonances ($J = 0,2,4,6$) close to EP(0,2). The upper panels show the absolute value Abs$(\Psi|J|\Psi)$, which, in field-free conditions, corresponds to the rotational quantum number J. The lower panels display the multivalued argument of $(\Psi|J|\Psi)$ for $J = 0$ and 2.

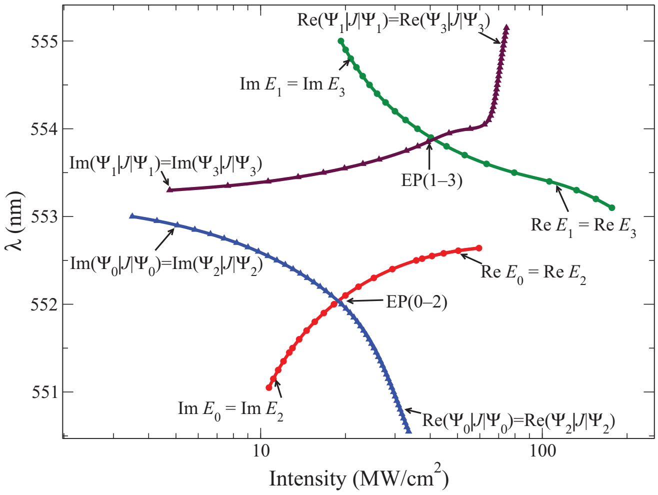

FIG. 11. (Color online) The loci of points where either the real or the imaginary parts of two observables [namely, (H), i.e., energy or (J), i.e., angular momentum] are identical, close to two EPs.

of $(\Psi_E|J|\Psi_E)$ for the resonances involved in the proximity of EP(0,2). Moreover, a sharp bifurcation with a vertical tangent occurs precisely at the position of EP(0,2), that is, at $\lambda^{\mathrm{EP}} = 552$ nm and $I^{\mathrm{EP}} = 20\ \mathrm{MW/cm^2}$. In the laser parameter plane, Fig. 11 displays the loci of points where either the real or the imaginary parts of two observables, energy or angular momentum $(\Psi_E|J|\Psi_E)$, are identical.

A comprehensive interpretation is provided by following the analysis given by Hernández *et al.* [45] for the bifurcation behavior close to an EP. We take, as the starting point, the identity on complex scalars $\mathcal{A}_\pm$,

$$\mathcal{A}_\pm \equiv \tfrac{1}{2}[\mathcal{A}_+ + \mathcal{A}_-] \pm \left[\tfrac{1}{4}(\mathcal{A}_+ - \mathcal{A}_-)^2\right]^{1/2}. \tag{12}$$

In Ref. [45], $\mathcal{A}$ describes the resonance complex energies dependent on two control parameters λ and I of the Hamiltonian. The derivation presented below is generic enough to accommodate any observable $\mathcal{A}$ (not limited to energies). We are looking for such conditions when there is either an equality of the real (Re) parts of $\mathcal{A}_\pm$ or of their imaginary (Im) parts. We assume, to be close enough to the EP, $(\mathcal{A}_+ \simeq \mathcal{A}_-)$ to validate a Taylor expansion of

$$\epsilon_\pm = \pm\left[\tfrac{1}{4}(\mathcal{A}_+ - \mathcal{A}_-)^2\right]^{1/2}. \tag{13}$$

Following Ref. [45], we write an approximation to $\epsilon_\pm$ as

$$\tilde{\epsilon}_\pm = \pm\sqrt{\tfrac{1}{4}[C_\lambda(\lambda - \lambda^{\mathrm{EP}}) + C_I(I - I^{\mathrm{EP}})]}. \tag{14}$$

Introducing three column vectors,

$$\vec{\xi} = \begin{pmatrix} \xi_1 \\ \xi_2 \end{pmatrix} = \begin{pmatrix} \lambda - \lambda^{EP} \\ I - I^{EP} \end{pmatrix}, \quad \vec{\mathbf{R}} = \mathrm{Re}\begin{pmatrix} C_1 \\ C_2 \end{pmatrix},$$
$$\vec{\mathbf{I}} = \mathrm{Im}\begin{pmatrix} C_1 \\ C_2 \end{pmatrix}, \tag{15}$$

an analysis of the splitting between $\mathcal{A}_\pm$ shows that the real and imaginary parts, respectively, of the observables (i.e., resonance energies in Ref. [45] or average values of J) close to the EP differ by

$$\mathrm{Re}(\tilde{\epsilon}_\pm) = \pm\frac{1}{2\sqrt{2}}[a(\lambda, I, C_\lambda, C_I) + \vec{R}\cdot\vec{\xi}\,]^{1/2}, \tag{16}$$

and

$$\mathrm{Im}(\tilde{\epsilon}_\pm) = \pm\frac{1}{2\sqrt{2}}[a(\lambda, I, C_\lambda, C_I) - \vec{R}\cdot\vec{\xi}\,]^{1/2}, \tag{17}$$

where

$$a(\lambda, I, C_\lambda, C_I) = \sqrt{(\vec{R}\cdot\vec{\xi})^2 + (\vec{I}\cdot\vec{\xi})^2}. \tag{18}$$

The cancellation of the difference $\tilde{\epsilon}_\pm$ (i.e., the fulfillment of the coalescence condition) is obtained by a specific choice of two unit vectors $\vec{\xi}_R$ and $\vec{\xi}_I$ in the parameter plane. More precisely, the real parts [Eq. (16)] are canceled with the choice,

$$\vec{I}\cdot\vec{\xi}_R = 0, \quad \vec{R}\cdot\vec{\xi}_R = -|\vec{R}\cdot\vec{\xi}_R|, \tag{19}$$

whereas, the imaginary parts [Eq. (17)] are canceled with the choice,

$$\vec{I}\cdot\vec{\xi}_I = 0, \quad \vec{R}\cdot\vec{\xi}_I = |\vec{R}\cdot\vec{\xi}_I|. \tag{20}$$

Finally, Eqs. (19) and (20) lead to the following important consequence:

$$\vec{\xi}_R = -\vec{\xi}_I. \tag{21}$$

The above equation means that the half-axis starting from the EP defined by $\vec{\xi}_R$ is a branch cut for the real parts of the observable $\mathcal{A}$, whereas, the half-axis supported by $\vec{\xi}_I$ and lying in the opposite direction is a branch cut for their imaginary parts [39,45]. Finally, the common point of these two half-axes is precisely the EP where both real and imaginary parts are equal. Figure 11 illustrates this interesting situation around two EPs, namely, EP(0,2) and EP(1,3), both for resonance energies and for angular momenta. Two observations are in order: (i) As the laser parameters scan regions far from the EP's positions, the loci corresponding either to the real or to the imaginary parts of the observables are no longer straight lines as resulting from the first-order Taylor expansion but are slowly varying curves [Eq. (14)]; (ii) most importantly, the two observables follow a similar behavior as expected from the generic model with a common EP position but different trajectories as resulting from different vectors $\vec{R}$ and $\vec{I}$ of Eq. (15).

IX. CONCLUSIONS AND PERSPECTIVES

We have shown that EPs also occur in laser-induced molecular rotational dynamics with important implications in control scenarios. We have accurately calculated their positions in the illustrative case of a Na_2 molecule referring to two different (gridlike versus baselike) numerical techniques for solving the Floquet Hamiltonian with Siegert-type boundary conditions. Moreover, we have shown that, as in the reduced one-dimensional model dealing with pure vibrational dynamics, rotational EPs are also organized by small clusters in the wavelength-intensity parameter plane. Such clusters make the control of the rotational population transfer more flexible, offering scenarios for improved robustness: For example, for the rotational cooling, one can use either successive laser pulses enclosing a single EP at a time or a single pulse enclosing a cluster of EPs with much improved robustness. We have also discussed the robustness of the proposed rotational transfer technique with respect to adiabaticity conditions. The adiabaticity of the laser pulse is itself a prerequisite of the applicability of the Floquet formalism. Even for very slowly varying laser parameters (which result in a weaker robustness of the technique because more molecules would dissociate for longer pulses), it turns out that the proximity of an EP may be expected to constitute a limitation to adiabaticity. The limitation is mainly due to a nonadiabatic mixing between resonances having significantly different lifetimes. Fortunately, a recently published detailed analysis on $H_2{}^+$ vibrational cooling has clearly shown the possibility to overcome these resonance overlaps by an optimal choice of laser loops aiming at a single resonance following and leading to exploitable robustness (i.e., better than 20% in this specific case) [20]. Our expectation (supported by some preliminary results) is the achievement of similar (or even better) robustness in the case of rotational transfers in Na_2, presumably in relation with much more adiabatic pulse characteristics than in the case of $H_2{}^+$. Finally, we have extended the discussion to the role of EPs on observables different than energy, namely, the average value of the angular momentum. To the best of our knowledge, this constitutes a proof of the bifurcation behavior, close to an EP, for different observables and gives additional insight in the theory.

In our group, further work is in progress to optimally control the laser shaping to take better advantage of the EPs in the rotational cooling strategy.

ACKNOWLEDGMENTS

One of us (O.A.) thanks Dr. E. Shapiro from the University of British Columbia for fruitful discussions. We acknowledge support from the EU (Project No. ITN-2010-264951, CORINF) and the National Science Foundation, Grant No. PHY-10-68785.

---

[1] S. Ospelkaus, K.-K. Ni, M. H. G. de Miranda, B. Neyenhuis, D. Wang, S. Kotochigova, P. S. Julienne, D. S. Jin, and J. Ye, Faraday Discuss. **142**, 351 (2009).
[2] J. G. Danzl, M. J. Mark, E. Haller, M. Gustavsson, R. Hart, J. Aldegunde, J. M. Hutson, and H.-C. Nägerl, Nat. Phys. **6**, 265 (2010).
[3] P. F. Staanum, K. Højbjerre, P. S. Skyt, A. K. Hansen, and M. Drewsen, Nat. Phys. **6**, 271 (2010).
[4] T. Schneider, B. Roth, H. Duncker, I. Ernsting, and S. Schiller, Nat. Phys. **6**, 275 (2010).
[5] M. Viteau, A. Chotia, M. Allegrini, N. Bouloufa, O. Dulieu, D. Comparat, and P. Pillet, Science **321**, 232 (2008).
[6] K. M. Jones, E. Tiesinga, P. D. Lett, and P. S. Julienne, Rev. Mod. Phys. **78**, 483 (2006).
[7] O. Atabek, R. Lefebvre, M. Lepers, A. Jaouadi, O. Dulieu, and V. Kokoouline, Phys. Rev. Lett. **106**, 173002 (2011).
[8] T. Kato, *Perturbation Theory for Linear Operators* (Springer-Verlag, Berlin, 1995).
[9] W. D. Heiss, Czech. J. Phys. **54**, 1091 (2004).
[10] I. Rotter, J. Phys. A: Math. Theor. **42**, 153001 (2009).
[11] N. Moiseyev, *Non Hermitian Quantum Mechanics* (Cambridge University Press, Cambridge, UK, 2011).
[12] M. V. Berry, Czech. J. Phys. **54**, 1039 (2004).
[13] M. Liertzer, L. Ge, A. Cerjan, A. D. Stone, H. E. Türeci, and S. Rotter, Phys. Rev. Lett. **108**, 173901 (2012).
[14] O. Latinne, N. J. Kylstra, M. Dörr, J. Purvis, M. Terao-Dunseath, C. J. Joachain, P. G. Burke, and C. J. Noble, Phys. Rev. Lett. **74**, 46 (1995).
[15] H. Cartarius, J. Main, and G. Wunner, Phys. Rev. Lett. **99**, 173003 (2007).
[16] A. Thilagam, J. Chem. Phys. **136**, 065104 (2012).
[17] M. Avinun-Kalish, M. Heiblum, O. Zarchin, D. Mahalu, and V. Umansky, Nature (London) **436**, 529 (2005).
[18] R. Lefebvre, O. Atabek, M. Šindelka, and N. Moiseyev, Phys. Rev. Lett. **103**, 123003 (2009).
[19] S. G. Schirmer, Phys. Rev. A **63**, 013407 (2000).
[20] A. Jaouadi, M. Desouter-Lecomte, R. Lefebvre, and O. Atabek, J. Phys. B **46**, 145402 (2013).
[21] F. K. Fatemi, K. M. Jones, P. D. Lett, and E. Tiesinga, Phys. Rev. A **66**, 053401 (2002).
[22] D. A. Varshalovich, A. N. Moskalev, and V. K. Khersonskii, *Quantum Theory of Angular Momentum* (World Scientific, Singapore, 1988).
[23] O. Atabek, R. Lefebvre, C. Lefebvre, and T. T. Nguyen-Dang, Phys. Rev. A **77**, 043413 (2008).
[24] M. Chrysos, O. Atabek, and R. Lefebvre, Phys. Rev. A **48**, 3845 (1993).
[25] S. Magnier, P. Millié, O. Dulieu, and F. Masnou-Seeuws, J. Chem. Phys. **98**, 7113 (1993).
[26] M. Aymar and O. Dulieu, J. Chem. Phys. **122**, 204302 (2005).
[27] R. Kosloff, J. Phys. Chem. **92**, 2087 (1988).
[28] D. T. Colbert and W. H. Miller, J. Chem. Phys. **96**, 1982 (1992).
[29] V. Kokoouline, O. Dulieu, R. Kosloff, and F. Masnou-Seeuws, J. Chem. Phys. **110**, 9865 (1999).
[30] V. Kokoouline, O. Dulieu, R. Kosloff, and F. Masnou-Seeuws, Phys. Rev. A **62**, 032716 (2000).
[31] R. B. Lehoucq, D. C. Sorensen, and C. Yang, ARPACK *Users' Guide: Solution of Large-Scale Eigenvalue Problems with Implicitly Restarted Arnoldi Methods* (SIAM, Philadelphia, 1997).
[32] N. Moiseyev, Phys. Rep. **302**, 212 (1998).
[33] O. Atabek, R. Lefebvre, and T. T. Nguyen-Dang, in *Handbook of Numerical Analysis*, edited by C. Le Bris (Elsevier, New York, 2003), Vol. X.
[34] L. Fox and E. T. Goodwin, Philos. Trans. R. Soc. London, Ser. A **246**, 1 (1953).
[35] A. F. J. Siegert, Phys. Rev. **56**, 750 (1939).
[36] O. Atabek, R. Lefebvre, and M. Jacon, J. Phys. B **15**, 2689 (1982).
[37] R. Lefebvre and O. Atabek, J. Mol. Mod. **19**, 1959 (2012).

[38] R. Lefebvre, A. Jaouadi, O. Dulieu, and O. Atabek, Phys. Rev. A **84**, 043428 (2011).
[39] E. Hernández, A. Jáuregui, and A. Mondragón, J. Phys. A **39**, 10087 (2006).
[40] R. Lefebvre, A. Jaouadi, and O. Atabek, Chem. Phys. **399**, 111 (2012).
[41] R. Uzdin, A. A. Mailybaev, and N. Moiseyev, J. Phys. A: Math. Theor. **44**, 435302 (2011).
[42] M. V. Berry and R. Uzdin, J. Phys. A: Math. Theor. **44**, 435303 (2011).
[43] I. Gilary and N. Moiseyev, J. Phys. B **45**, 051002 (2012).
[44] A. Jaouadi, M. Desouter-Lecomte, R. Lefebvre, and O. Atabek, Fortschr. Phys. **61**, 162 (2013).
[45] E. Hernández, A. Jáuregui, and A. Mondragón, Phys. Rev. E **72**, 026221 (2005).